

# Differential and Persistent Scatterer SAR Interferometry

## .. DInSAR & PS-InSAR

Karlis Zalite and Kaupo Voormansik

June 17, 2016



**TARTU OBSERVATORY**  
space research centre

## 1 SAR basics

### 1.1 Introduction

Synthetic aperture radar (SAR) is an active, coherent, microwave imaging remote sensing system that can be mounted on an airborne or a spaceborne platform. In this document, however, we will deal with the spaceborne case only. The four terms mentioned in the SAR definition above help to understand the principles of SAR and are described below.

**Imaging.** An imaging system forms a digital image of the observed area. It provides information how the recorded signal varies in space, not just in strength.

**Active.** SAR systems carry their own illumination, i.e. the antenna that serves as both the transmitter and the receiver. The outcome of such a configuration is that SAR can provide meaningful images in the absence of sunlight.

**Coherent.** Coherent systems can record not only the amplitude of the received signal but also the phase. Thus, a pixel in a SAR image can contain information about the strength of the signal as well as its phase. The notation is expanded in Section 1.7.

**Microwave.** SAR operates in the microwave domain, i.e. it uses wavelengths from  $\approx 1$  cm to  $\approx 1$  m. The wavelengths that are operated most often are discussed in Section 1.5. The immediate benefit of using microwaves is that the signal can penetrate clouds (providing images independent of weather) and other media, such as vegetation, for example.

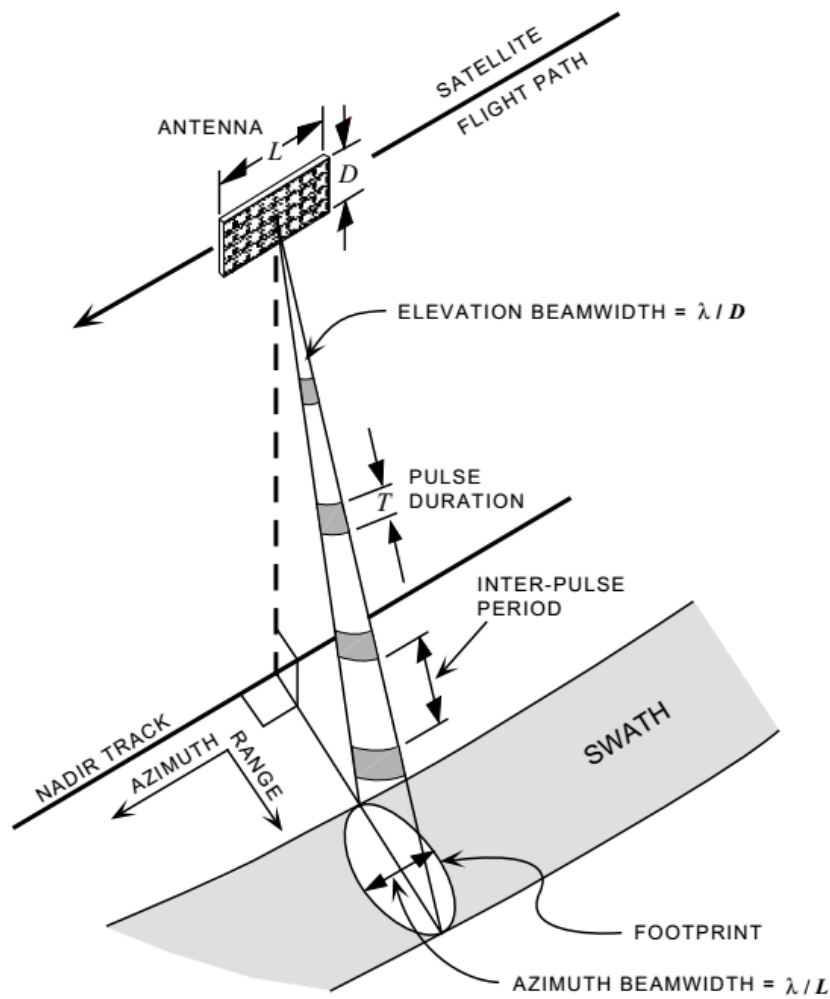


Figure 1: Configuration of a side-looking SAR system. Image from [1].

## 1.2 Geometry

The general configuration of a side-looking SAR system is given in Figure 1. The antenna is mounted on a platform moving in the along track (azimuth) direction, and the movement provides scanning in the azimuth direction. The radar beam is directed to the side and towards the surface. The dimensions of the antenna (height  $D$  and width  $L$ ) together with the wavelength  $\lambda$  define the footprint on the ground. The radar pulses are returned from the area within the footprint with the time of return depending on the pixel placement in the range direction. Thus, analyzing the time of return of separate pulses provides scanning in the range direction.

### 1.3 Resolution

**Range resolution.** A geometrical explanation of the range resolution is given in Figure 2. Range resolution is governed by pulse length  $\tau$  that is defined as  $1/B$  where  $B$  is bandwidth. Thus, resolution in range direction improves with increasing bandwidth.

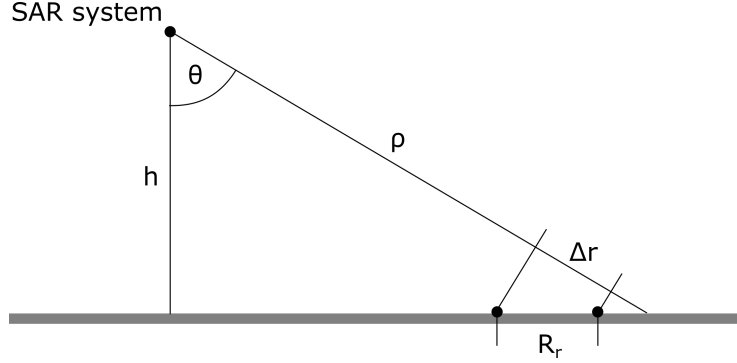


Figure 2: Resolution in the range direction, front view.

where

- $\theta$  – look angle
- $h$  – platform height
- $B$  – bandwidth of the system
- $\tau$  – pulse length,  $1/B$
- $C$  – speed of light
- $\rho$  – nominal slant range,  $h/\cos\theta$

Resolution in the slant range is given as:

$$\Delta r = \frac{C\tau}{2}, \quad (1)$$

and in the ground range as:

$$R_r = \frac{C\tau}{2} \frac{1}{\sin\theta}. \quad (2)$$

**Azimuth resolution.** In the azimuth direction, the resolution is defined by the width of the antenna,  $L$ . The footprint (in azimuth direction)  $L_{eff}$  of beam at range  $\rho$  is

$$L_{eff} = \frac{\lambda\rho}{L} \quad (3)$$

and this parameter indicates the amount of surface illuminated by the SAR pulse.  $L_{eff}$  represents the effective aperture of the moving radar. It is the distance traveled by the antenna while the target is within the beam, so that all pulses emitted during this time contribute some information about the target backscatter [1]. Thus, the larger this aperture, the more information is gathered

about the target while the platform is moving. This is the principle of synthetic aperture. The azimuth resolution for a SAR system is then given as:

$$R_a = \frac{\lambda \rho}{2L_{eff}} = \frac{\lambda \rho}{2 \frac{\lambda R}{L}} = \frac{L}{2}. \quad (4)$$

The azimuth resolution is independent of spacecraft orbital altitude and improves as the antenna length is reduced.

## 1.4 Geometric distortions

Due to the fact that pixel spacing in the range direction is governed by the time of return, there are geometric distortions present on SAR images, see Figure 3. The three distortions are foreshortening, layover, and shadowing. An example of these distortions is given in Figure 4 where an image of the Giza pyramid complex is given.

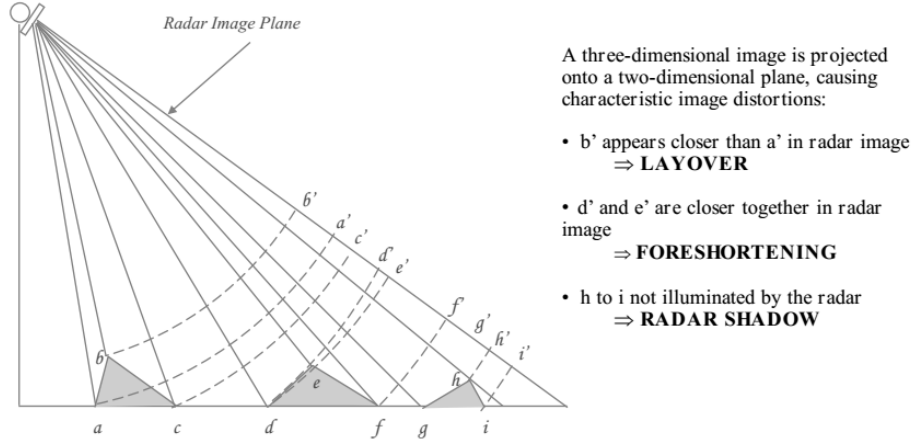


Figure 3: Geometric distortions of a SAR system. Image from caltech.edu.

## 1.5 Wavelength

As mentioned before, the microwave domain usually refers to wavelength from  $\approx 1$  cm to  $\approx 1$  m. In reality SAR systems use several predefined wavelength bands. The most often used bands and spaceborne systems that use them are given in Table 1.

Band	Wavelength	Frequency	SAR system(s)
X	$\approx 3.1$ cm	$\approx 9.6$ GHz	TanDEM-X, COSMO-SkyMed
C	$\approx 5.6$ cm	$\approx 5.4$ GHz	Sentinel-1, Radarsat-2
L	$\approx 23.5$ cm	$\approx 1.3$ GHz	ALOS PALSAR 2
P	$\approx 70.0$ cm	$\approx 0.4$ GHz	BIOMASS

Table 1: Often-used wavelengths



Figure 4: A Sentinel-1 image of the Giza pyramid complex. The two larger pyramids are clearly visible in the center. The foreshortening of the pyramid peaks can be observed, as well as the shadowing.

## 1.6 Polarization

The electric component of an electromagnetic (EM) wave can oscillate in any direction normal (perpendicular) to the direction of wave propagation. In the case of SAR, two basic polarizations are used: horizontal or H, and vertical or V. When describing a SAR system, a double notation is used, e.g. HH, HV, VV, or VH. If the system mode is described as HH polarized, it means that it emits H wave and receives H wave as well. On the other hand, in the case of VH, V signal is emitted but H is recorded. Such a system would be sensitive to targets that change the polarization of a SAR signal, such as vegetation. SAR systems can be fully polarimetric, i.e. provide data recorded in all possible polarization modes HH, HV, VH, and VV. However, most systems provide not fully polarimetric data. For example, the usual mode for Sentinel-1 provides VH and VV data. The choice of which polarization to use for data analysis depends on the target under investigation.

## 1.7 Complex notation

As mentioned before, SAR is a coherent instrument, i.e. it records signal phase as well as amplitude. A Level-1 SAR data is stored as a complex number comprising two channels:  $I$  and  $Q$ . These channels can be used to reconstruct the amplitude and the phase of the recorded signal, see Figure 5. The amplitude of the signal is given as:

$$|z| = \sqrt{I^2 + Q^2} \quad (5)$$

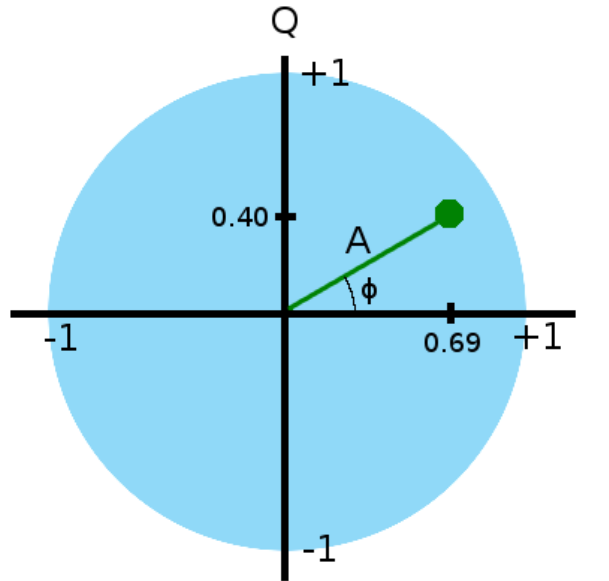


Figure 5: The complex notation. Image from <http://whiteboard.ping.se>.

And the phase:

$$\arg(z) = \phi = \tan^{-1} \left( \frac{Q}{I} \right) \quad (6)$$

For the signal in Figure 5, the amplitude is then  $\sqrt{0.68^2 + 0.40^2} = 0.8$ , and the phase  $+30^\circ$ .

## 1.8 Speckle

Speckle is a noise-like characteristic caused by the coherent nature of a SAR system. Physical objects in the resolution cell on the ground all contribute to the returned SAR signal. The contributions are then coherently summed up and the final contribution of the cell is formed. The summation can be high in case of constructive interference or low in case of destructive interference. The speckle can be filtered using different methods. For a comprehensive overview of these methods, please refer to [2]. An example of an unfiltered and filtered SAR image is given in Figure 6.

## 2 InSAR principles

### 2.1 InSAR geometry

Consider Figure 7 that shows the difference in positioning the returned signal in case of a single antenna (left) and interferometric SAR setup (right). Due to the way how resolution is achieved in the range direction, it is impossible to estimate the target's altitude or position in the 3rd dimension ( $z$ ) from a single antenna

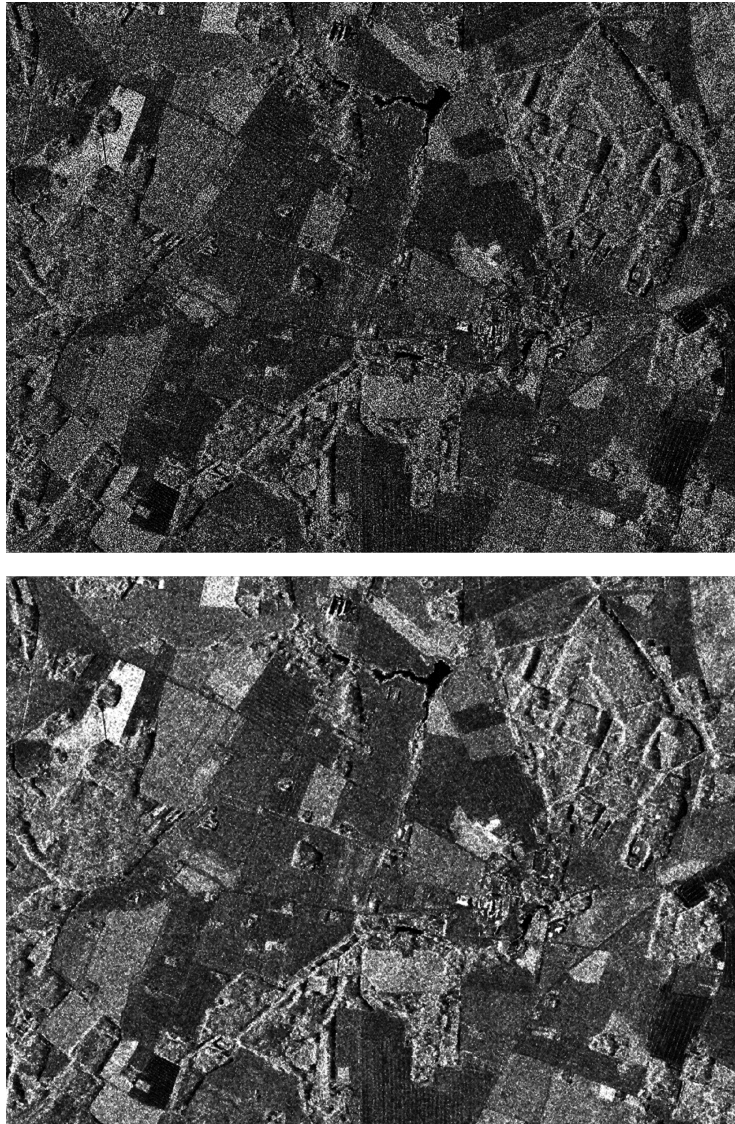


Figure 6: A TerraSAR-X image of an agricultural area in Rannu, Estonia: (top) unfiltered image; (bottom) speckle filtered image.

setup. However, when a second antenna separated from the first one with a baseline  $B$  is introduced creating an interferometric (InSAR) setup, resolution in the third dimension can be gained. When interferometry is performed, we exploit the phase information of two or more SAR images.

## 2.2 Phase difference contributions

InSAR is based on the computation of the complex correlation coefficient:

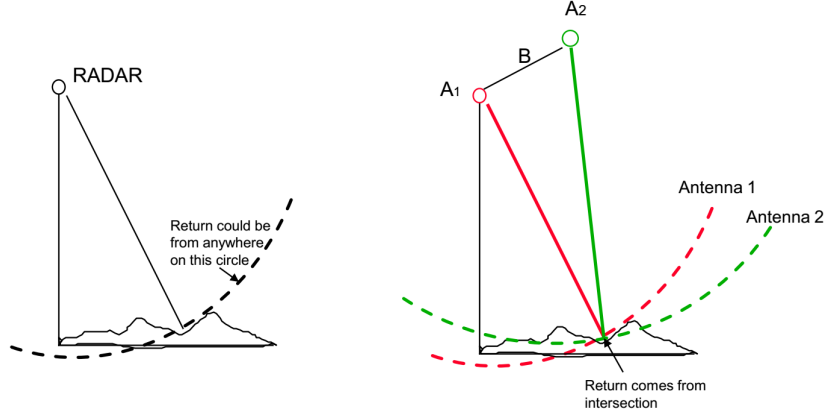


Figure 7: Basic principle of interferometric SAR. Image from caltech.edu.

$$\gamma = \frac{\langle s_1 s_2^* \rangle}{\sqrt{\langle s_1 s_1^* \rangle \langle s_2 s_2^* \rangle}}, \quad 0 \leq |\gamma| \leq 1, \quad (7)$$

where  $s_1$  and  $s_2$  are two complex images in the interferometric pair,  $\langle \dots \rangle$  denotes an averaging operation, and  $*$  denotes a complex conjugate product. The amplitude of the complex correlation coefficient  $|\gamma|$  is the interferometric coherence and is discussed in the following subsection. On the other hand, the phase or the argument of the coefficient  $\arg(\gamma)$  is the phase difference  $\Delta\phi$  between the InSAR acquisitions that has multiple contributions:

$$\Delta\phi = \Delta\phi_{flat} \Delta\phi_{elevation} \Delta\phi_{displacement} \Delta\phi_{atmosphere} \Delta\phi_{noise}, \quad (8)$$

where

$$\Delta\phi_{flat} = -\frac{4\pi}{\lambda} \frac{B_n s}{R \tan \theta} \quad (9)$$

$$\Delta\phi_{elevation} = -\frac{\Delta q}{\sin \theta} \frac{B_n}{R} \frac{4\pi}{\lambda} = 2\pi \frac{\Delta q}{h_a} \quad (10)$$

$$\Delta\phi_{displacement} = +\frac{4\pi}{\lambda} d, \quad (11)$$

where the variables are given in Table 2.

$\lambda$	wavelength
$B_n$	perpendicular baseline
$s$	ground range to the target
$R$	radar-target distance
$\theta$	incidence angle
$\Delta q$	relative elevation (to flat earth)
$h_a$	height of ambiguity
$d$	displacement independent of the baseline

Table 2: Variables used in InSAR calculations.

$\Delta\phi_{atmosphere}$  phase variations are caused by atmosphere, and  $\Delta\phi_{noise}$  is induced by the physical setup of the system and the data processing accuracy. These terms are not related to the target and will not be discussed in length. For further information, please refer to [3]. The  $\Delta\phi_{flat}$ ,  $\Delta\phi_{elevation}$ , and  $\Delta\phi_{displacement}$  terms are further in detail in the following subsections.

### 2.2.1 Flat earth phase $\Delta\phi_{flat}$

The  $\Delta\phi_{flat}$  term is a phase variation proportional to the slant range displacement  $s$  of the point targets, i.e. it is caused by variations in the range positions of individual pixels. An example of how the FE influences an interferogram (visual representation of the interferometric phase) is given in Figure 8. The FE removal is a mandatory step in InSAR processing.

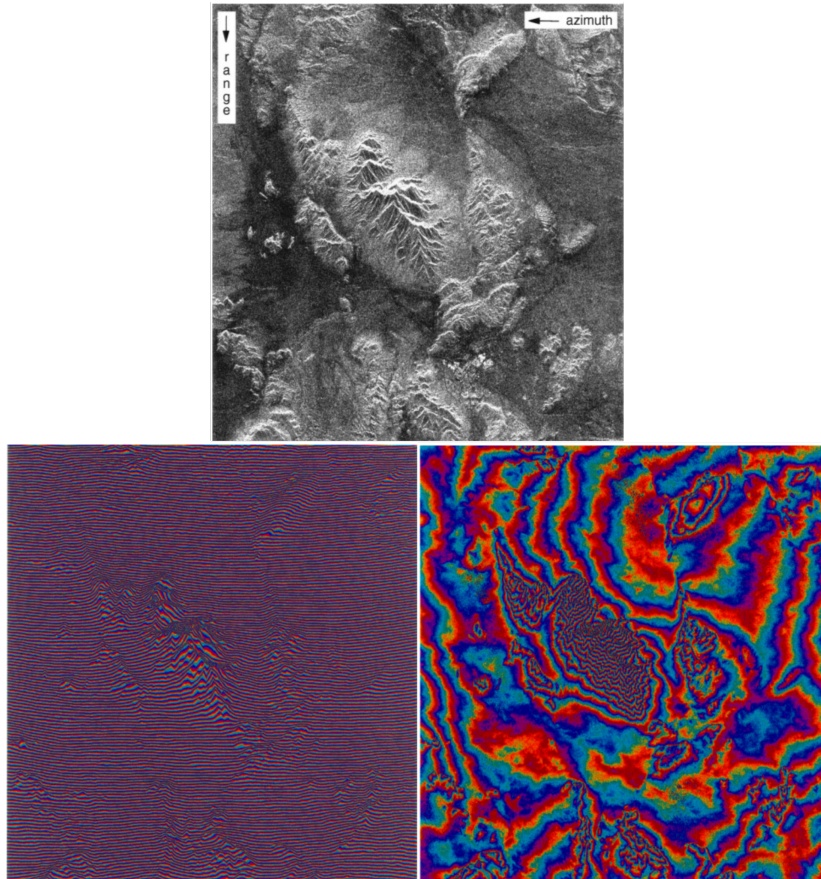


Figure 8: **(top)** SAR magnitude image of an area in Mojave desert. **(bottom-left)** An interferogram of the same area before FE removal. Interferometric phase in color wheel representation. Sensor: ERS-1/2. Baseline:  $B_n = 133\text{ m}$ . **(bottom-right)** Interferogram after FE removal. Now, the topographic phase  $\Delta\phi_{elevation}$  is visible more clearly. Images from [3].

### 2.2.2 Topography phase $\Delta\phi_{elevation}$

The elevation term  $\Delta\phi_{elevation}$  allows to create DEMs and DTMs from InSAR data but it is dependent on the baseline  $B_n$ . The larger the baseline, the smaller variations in the topography can be detected. However, there exists a critical baseline  $B_{crit}$  that, if exceeded, leads to total decorrelation of the signal and loss of interferometric resolution.

Sensitivity of the InSAR system to elevation is, as mentioned before, governed mainly by the baseline, and it can be described as height of ambiguity:

$$h_a = \frac{\lambda R \sin \theta}{2B_n}, \quad (12)$$

that defines the 'fringe' of the interferogram (e.g. elevation change between one blue line to another blue line). Any InSAR system is capable of measuring elevation within the range of  $2\pi$ . In order to 'connect' the measurements and create a realistic interpretation of the elevation, phase unwrapping is needed, see Figure 9. For more information about the topic please see [5], Chapter 11.

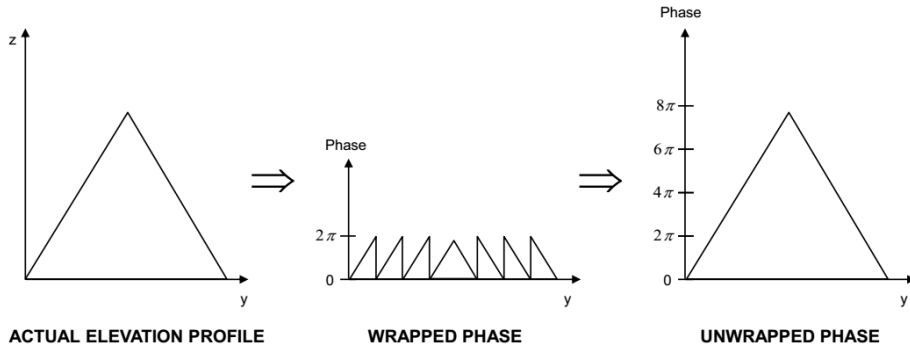


Figure 9: Phase unwrapping. Image from caltech.edu.

### 2.2.3 Change in topography $\Delta\phi_{displacement}$

If the  $\Delta\phi_{flat}$  and  $\Delta\phi_{elevation}$  terms have been subtracted from the measure  $\Delta\phi$ , one last term related to the target is the displacement term  $\Delta\phi_{displacement}$ . It describes the baseline-independent target's change in position between the InSAR acquisitions, see Figure 10.

Measurement of the  $\Delta\phi_{displacement}$  is referred to as differential SAR interferometry or DInSAR. An example of the approach is showed in Figure 11. Here, a synthetic interferogram (e.g. derived from a DTM) is subtracted from the flattened interferogram, yielding the underlying displacement information in the form of a differential interferogram.

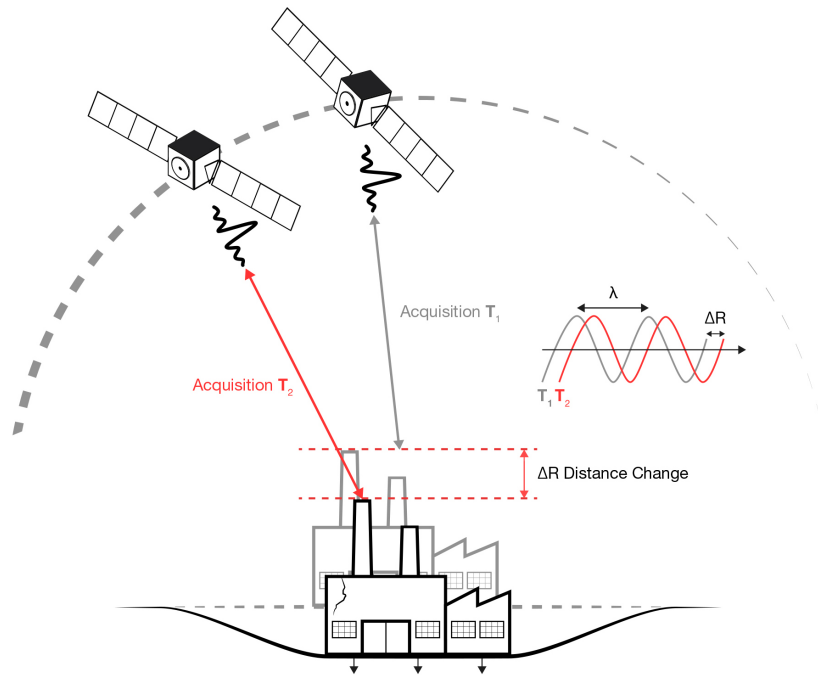


Figure 10: The measured displacement. Image from <http://effigis.com/>.

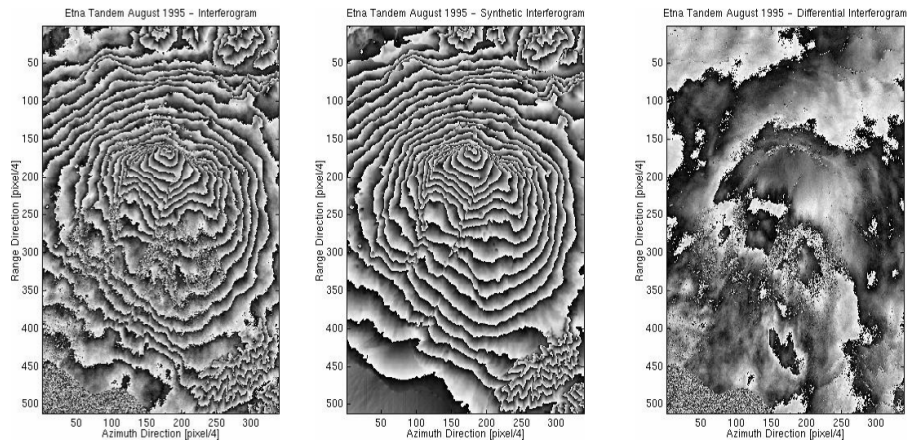


Figure 11: DInSAR example. **(left)** Flattened interferogram. **(middle)** Synthetic interferogram, e.g. derived from a DTM. **(right)** Result of subtracting the **(middle)** from **(left)**, shows displacements in the surface of a volcano that occurred between the acquisitions used to create the original interferogram. Image from [4].

### 2.3 Coherence, decorrelation sources

Interferometric coherence is a measure of the phase noise and phase precision. Coherence is a normalised parameter with values between 1 and 0. The higher

the coherence, the less noise and the phase measurement can be trusted more. There are several sources of decorrelation that can be distinguished as (from [6]):

- baseline or geometric decorrelation ( $\gamma_{geom}$ ), caused by the difference in the incidence angles between two acquisitions;
- Doppler centroid decorrelation ( $\gamma_{DC}$ ), caused by differences in the Doppler centroids between two acquisitions;
- volume decorrelation ( $\gamma_{vol}$ ), caused by penetration of the radar wave in the scattering medium;
- thermal or system noise ( $\gamma_{SNR}$ ), caused by the characteristics of the system, including gain factors and antenna characteristics;
- temporal decorrelation ( $\gamma_{temporal}$ ), caused by physical changes in the target, affecting the scattering characteristics, and
- processing induced decorrelation ( $\gamma_{processing}$ ), which results from the chosen algorithms, e.g. coregistration and interpolation, and
- estimation bias decorrelation ( $\gamma_{bias}$ ), caused by the choice of averaging window in (7).

The estimation of each of these terms is described in detail in [6]. An example of the influence of coherence on interferometric phase is given in Figure 12. The topic of coherence is essential for successful application of DInSAR and PSInSAR, and it is discussed more in the respective sections.

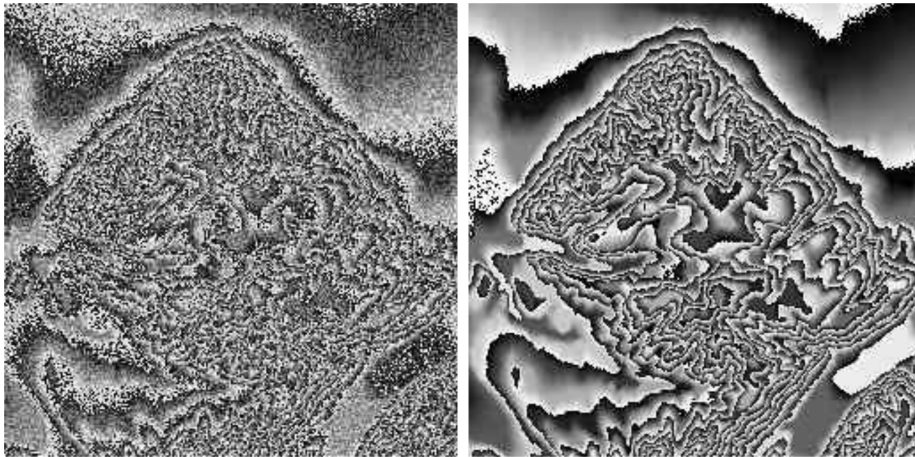


Figure 12: Effect of coherence on the interferometric phase. Phase image when coherence is low (**left**) and high (**right**). Low coherence makes unattractive, noisy interferograms. Often, these interferograms are difficult to phase unwrap. Image from ESA.

### 3 DInSAR

This section is mainly based on [7].

'Differential interferometry' is the commonly used term for the production of interferograms from which the topographic contribution has been removed. However, the term may occasionally be misleading, because on the one hand interferometry is a differential technique right from the beginning, and on the other hand, the subtraction process can be pushed further as well as in other directions (e.g. subtraction of an expected geophysical contribution through earthquake or volcano dynamic modelling).

To repeat, the interferometric phase after the flat earth subtraction is:

$$\Delta\phi = -\frac{4\pi}{\lambda} \frac{B_n \Delta q}{R \sin \theta} + \frac{4\pi}{\lambda} d \quad (13)$$

There are several ways of producing a differential interferogram:

1. **Single interferometric pair and near-zero baseline.** With a single interferometric pair (two SAR images) and baseline  $B_n$  close to zero: the interferometric phase contains the motion contribution only (see Equation 13). No other processing steps are required.
2. **Single interferometric pair and non-zero baseline.** With a single interferometric pair (two SAR images) and non-zero baseline: the interferometric phase contains both altitude and motion contributions. The following processing steps are required:
  - (a) An available DEM must be re-sampled from geographic to SAR coordinates and the elevation must be converted into interferometric phases by inverting Equation 13. The same baseline should be used as for the interferometric pair.
  - (b) These 'synthetic' fringes should be subtracted from those of the available interferometric pair. Notice that this operation can be conveniently done in the complex domain by multiplying the actual interferogram by the complex conjugate of the synthetic one.
3. **Three interferometric images and no motion.** With three interferometric SAR images and no terrain motion between two of them, one image should be selected as a common master. Two interferograms are then formed: the two slave images are registered to the common master.

The shortest temporal difference (to gain coherence and avoid terrain motion) and a medium/high baseline (to gain elevation accuracy) should be selected for the first interferometric pair. The second pair should have a larger temporal difference (it should contain the terrain motion) and a short baseline.

The following processing steps are required:

- (a) The first interferogram should be unwrapped and scaled by the ratio of the two baselines.
- (b) Its phase should be wrapped again and subtracted from that of the second interferogram (generally done in the complex domain as described in point 2 above).

However, if the baselines of the two pairs are in an integer ratio, no unwrapping is required. In this case the phases of one interferogram can be directly scaled by the integer ratio between baselines and subtracted from the phases of the other interferogram. The available collection of images should be analysed carefully to check if this very favourable condition can be met (phase unwrapping is still one of the most delicate points in SAR interferometry).

4. **Two image pairs and no motion in one of them.** With two interferometric pairs (four SAR images) and no terrain motion in one of them: there are two master images, each of them with a slave image. All the images should be registered to each other. We end up with two interferograms as in the case of three SAR images analysed in point 3, so the same steps are required.

Tips for image selection:

- Select either ascending or descending passes, depending on which will avoid foreshortening in the area of interest.
- Select those image pairs with the smallest perpendicular baseline in the required range of dates. Bear in mind that the smaller the baseline, the smaller the topography contribution to the interferometric phase. As a consequence, a less precise DEM will be required for the topography subtraction. Moreover, the smaller the baseline, the higher the expected coherence.
- Check first the possibility of using only three images: a tandem pair (for DEM generation) and a third image, acquired after the desired time interval, that shows a small perpendicular baseline with either the first or the second image of the selected tandem pair (to make a second interferometric pair).

### 3.1 Applications of DInSAR

The DInSAR technique can be applied in numerous situations, such as but not limited to monitoring of dams, glacier motion, volcanic activities, earthquake deformations, coastline erosion, underground mining and water extraction.

In Estonia, subsidence monitoring is of interest due to use of ground water, mining activities and post-glacier rebound in the Baltic sea area. Additionally, monitoring of infrastructure such as overpasses and bridges can be done as well.

An example of DInSAR over a mining area from [8] is given in Figure 13. Figure 13 shows the most active mining subsidence areas. More than 20 active areas are clearly identified in this interferogram, represented by closed circular shaped fringes. The location of these active areas (subsidence basins) corresponds with the location of coal mining areas, suggesting a clear relationship between the mining activity and measured deformation.

Monitoring of infrastructure, however, is most often done using PSInSAR – a technique similar to DInSAR. It is discussed in Section 4. An example of evaluating bridge displacement using PInSAR is given in Figure 14 [9].

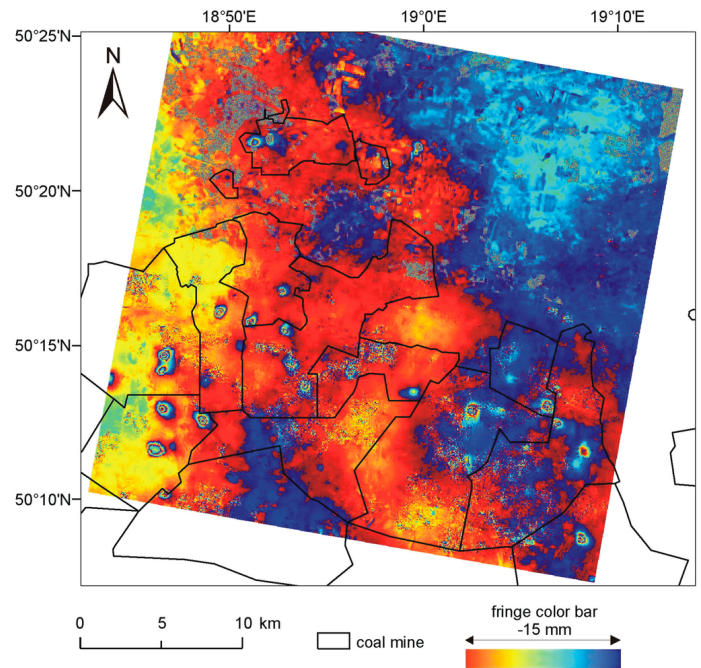


Figure 13: TerraSAR-X (TSX) X-band differential interferogram with boundaries of coal mining areas in Upper Silesia Coal Basin. Start and end dates of the interferogram are 25 November 2011–06 December 2011 [8].

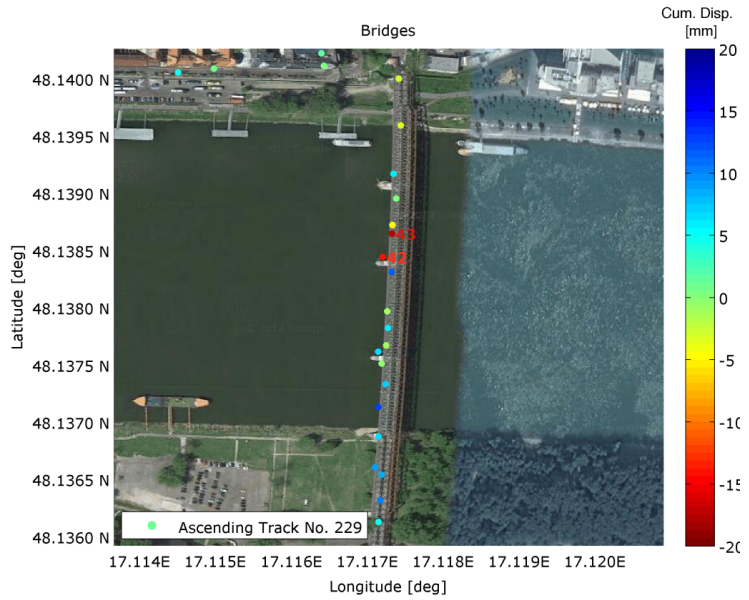


Figure 14: PSInSAR time series over a bridge that was affected by a tug crash [9].

## 4 PS-InSAR

This section is mainly based on [5].

As described before, the phase of a pixel in an interferogram indicates the summed result of topography and displacement of an observed target, associated atmospheric delay and other changes at the time of the acquisitions. Their individual phase components are superimposed in the interferogram. In some cases, the phase components of other changes can be practically neglected or independently estimated, and the interferometry is therefore successfully applied. However, in most cases, due to temporal and geometrical decorrelation, the phase unwrapping process is very difficult, usually even impossible. The permanent scatterer (PS) technique has been developed by Ferretti et al. [10] to overcome these problems. PS technique utilizes all archived but suitable data of a certain area, stacks differential interferograms co-registered to a common master one. Instead of analysing the phase in the spatial domain in the entire scene, the phase of isolated coherent points is analysed as a function of time and space, see Figure 15. The PS technique is protected by a patent of Ferretti et al. and the term “Permanent Scatterer Technique” is trademarked. Therefore many scientists use another term – “Persistent Scatterer Technique” – with the same idea but with some small differences [11].

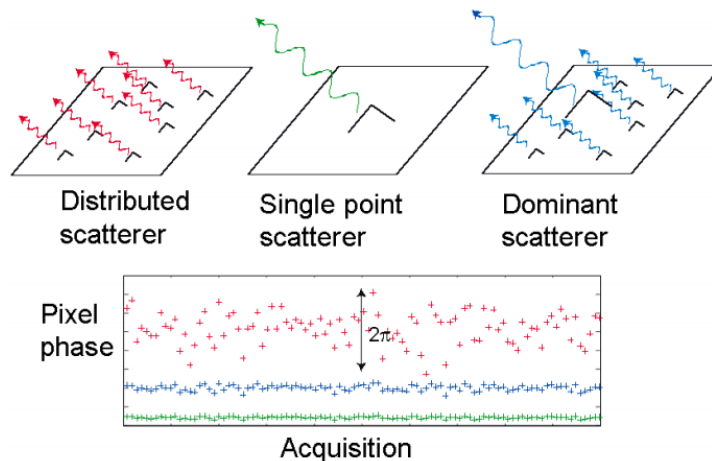


Figure 15: Scattering mechanism models for a SAR resolution element - distributed scatterers (red), ideal single point scatterer (green) and persistent scatterer (blue). The persistently scattering pixel exhibits smaller phase variation than the distributed scattering pixel [12].

All the available images from the chosen data set on the same track and frame must be co-registered to a master image. The master image is selected for decreasing the dispersion of the perpendicular baselines of all the possible interferometric combinations, and the acquisition time of the master image lies in or near the middle of the entire acquisition time range. In this course we use only Sentinel-1 images, so that the difference of Doppler centroid frequency is very small and therefore will not be considered. When the master image has been chosen, all the interferograms between the master image and slave images

will be generated.

A reference digital elevation model (DEM) and precise orbit data are used to obtain the simulated interferometric phase induced by topography. The differential interferograms are then generated by subtracting the simulated interferometric phase of topography from the interferograms. In fact, the interferometric phase of topography can be computed from a subset of the available images, preferably with large perpendicular and small temporal baselines, if these images are highly coherent everywhere (does not apply in the case of Sentinel-1).

#### 4.1 Mathematical principle [7]

Let us consider  $N$  differential interferograms computed between the selected slave images and one master. After DEM compensation, the residual phase of interferogram  $i$  is:

$$\phi_i = \frac{4\pi}{\lambda} r_{Ti} + \alpha_i + n_i + \epsilon_{topo.i} \quad (14)$$

where  $\lambda$  is the wavelength,  $\alpha_i$  is the atmospheric phase contribution,  $n_i$  is the decorrelation noise,  $\epsilon_{topo.i}$  is the phase contribution due to possible errors in the DEM (proportional to the normal baseline of each image  $B_{n.i}$ ), and  $r_{Ti}$  is the possible target motion in the direction of the satellite line-of-sight.

The first term in (14) can be written as follows:

$$\frac{4\pi}{\lambda} r_{Ti} = \frac{4\pi}{\lambda} v_r T_i + \mu_{NLi} = C_{\nu i} \nu + \mu_{NLi} \quad (15)$$

where  $\nu$  is the unknown component of the mean target velocity in the direction of the line of sight,  $\mu_{NL}$  is the phase term due to a possible non-linear target motion,  $T_i$  is the temporal baseline between the master acquisition and the generic  $i$ -th slave image.

Since we have  $N$  differential interferograms of the same area with different temporal and geometric baselines, we finally write, for each pixel, a linear system of  $N$  equations and two unknowns:

$$\phi_i = C_{zi} \epsilon_z + C_{\nu i} \nu, \quad i = 1..N \quad (16)$$

where  $\epsilon_z$  is the DEM error, and  $C_{zi}$  is proportional to  $B_{n.i}$ .

The problem would be linear if we knew the unwrapped phase values. However, using a simple periodogram (albeit with an irregular sampling of the two dimensions: baselines and time) we can estimate both the residual elevation and the mean line of sight velocity, provided that the signal-to-noise ratio is high enough.

Actually the Linear Phase Residues (LPR)  $w_i$  (i.e. phase data after linear detrending in temporal and spatial baseline) are the sum of three contributions: atmospheric components (Atmospheric Phase Screen – APS) of the master and the slave acquisitions, noise, and non-linear motion:

$$w_i = \phi_i - C_{zi} \epsilon_z - C_{\nu i} \nu = \mu_{NLi} + \alpha_i + n_i \quad (17)$$

Since  $\mu_{NL}$ ,  $\alpha$  and  $n$  are independent random variables, the residual phase variance  $\sigma_w^2$  is the sum of three contributions:  $\sigma_{\mu_{NL}}^2$ ,  $\sigma_{\alpha}^2$ ,  $\sigma_n^2$ . Proper estimation of target motion and elevation is possible only if  $\sigma_w^2$  is low, i.e. the target is

stable. To this end, the analysis is carried out in two steps. First a subset of image pixels is selected using the coherence maps of the area of interest: only locations of highly coherent targets are retained (low  $\sigma_n^2$ ). If now we consider a pair of targets not too far apart (distance less than, say, 1 km), it is usually possible to estimate  $\Delta\nu$  (relative mean velocity) and  $\Delta\epsilon_z$  (relative elevation error) with a high degree of accuracy. In fact, low distance implies low variance of the atmospheric component: for points less than 1 km apart, values of  $\sigma_\alpha^2$  less than  $0.1 \text{ rad}^2$  are common. Moreover, the motion of neighboring pixels is usually correlated. Estimation of  $(\nu, \epsilon_z)$  is then obtained by integrating the values of  $(\Delta\nu, \Delta\epsilon_z)$  previously estimated from pairs of neighboring pixels. Following this approach, we can actually unwrap the differential interferograms. In fact, if the condition  $|w_i| < \pi$  is satisfied, we can easily recover the unwrapped phase differences  $\Delta\phi_i$  between pairs of neighboring pixels and then integrate them all over the sparse grid of PS candidates.

## References

- [1] Olmsted, C. (1993). Alaska SAR Facility scientific SAR user's guide. University of Alaska Fairbanks, Geophysical Institute. ASF-SD-003.
- [2] Lee, J. S., & Pottier, E. (2009). Polarimetric radar imaging: from basics to applications. CRC press.
- [3] Bamler, R., & Hartl, P. (1998). Synthetic aperture radar interferometry. *Inverse problems*, 14(4), R1.
- [4] Rocca, F. DINSAR: Differential SAR Interferometry. Online at <http://earth.esa.int/landtraining07/D1LB5-1-Rocca.pdf> (as of 17 March 2015).
- [5] Xu, G. (Ed.). (2010). *Sciences of Geodesy*. Springer.
- [6] Hanssen, R. F. (2001). *Radar interferometry: data interpretation and error analysis (Vol. 2)*. Springer Science & Business Media.
- [7] Ferretti, A., Monti-Guarnieri, A., Prati, C., Rocca, F., & Massonet, D. (2007). *InSAR Principles-Guidelines for SAR Interferometry Processing and Interpretation (Vol. 19)*.
- [8] Przyłucka, M., Herrera, G., Graniczny, M., Colombo, D., & Bejar-Pizarro, M. (2015). Combination of conventional and advanced DInSAR to monitor very fast mining subsidence with TerraSAR-X Data: Bytom City (Poland). *Remote Sensing*, 7(5), 5300-5328.
- [9] Bakon, M., Perissin, D., Lazecky, M., & Papco, J. (2014). Infrastructure Non-Linear Deformation Monitoring Via Satellite Radar Interferometry. *Procedia Technology*, 16, 294-300.
- [10] Ferretti, A., Prati, C., & Rocca, F. (2001). Permanent scatterers in SAR interferometry. *Geoscience and Remote Sensing, IEEE Transactions on*, 39(1), 8-20.

- [11] Werner, C., Wegmüller, U., Strozzi, T., & Wiesmann, A. (2003, July). Interferometric point target analysis for deformation mapping. In *Geoscience and Remote Sensing Symposium, 2003. IGARSS'03. Proceedings. 2003 IEEE International* (Vol. 7, pp. 4362-4364). IEEE.
- [12] Agram, P. S. (2010). *Persistent scatterer interferometry in natural terrain* (Doctoral dissertation, stanford university).
- [13] Hooper, A., Zebker, H., Segall, P., & Kampes, B. (2004). A new method for measuring deformation on volcanoes and other natural terrains using InSAR persistent scatterers. *Geophysical research letters*, 31(23).